
This is an electronic reprint of the original article.
This reprint may differ from the original in pagination and typographic detail.

Author(s): Packard, R. E. & Pekola, Jukka & Price, P. B. & Spohr, R. N. R. & Westmacott, K. H. & Yu-Qun, Zhu

Title: Manufacture, observation, and test of membranes with locatable single pores

Year: 1986

Version: Final published version

Please cite the original version:

Packard, R. E. & Pekola, Jukka & Price, P. B. & Spohr, R. N. R. & Westmacott, K. H. & Yu-Qun, Zhu. 1986. Manufacture, observation, and test of membranes with locatable single pores. *Review of Scientific Instruments*. Volume 57, Issue 8. 1654-1660. ISSN 0034-6748 (printed). DOI: 10.1063/1.1138545.

Rights: © 1986 AIP Publishing. This is the accepted version of the following article: Packard, R. E. & Pekola, Jukka & Price, P. B. & Spohr, R. N. R. & Westmacott, K. H. & Yu-Qun, Zhu. 1986. Manufacture, observation, and test of membranes with locatable single pores. *Review of Scientific Instruments*. Volume 57, Issue 8. 1654-1660. ISSN 0034-6748 (printed). DOI: 10.1063/1.1138545, which has been published in final form at <http://scitation.aip.org/content/aip/journal/rsi/57/8/10.1063/1.1138545>

All material supplied via Aaltodoc is protected by copyright and other intellectual property rights, and duplication or sale of all or part of any of the repository collections is not permitted, except that material may be duplicated by you for your research use or educational purposes in electronic or print form. You must obtain permission for any other use. Electronic or print copies may not be offered, whether for sale or otherwise to anyone who is not an authorised user.

Manufacture, observation, and test of membranes with locatable single pores

R. E. Packard, J. P. Pekola, P. B. Price, R. N. R. Spohr, K. H. Westmacott, and Zhu Yu-Qun

Citation: [Review of Scientific Instruments](#) **57**, 1654 (1986); doi: 10.1063/1.1138545

View online: <http://dx.doi.org/10.1063/1.1138545>

View Table of Contents: <http://scitation.aip.org/content/aip/journal/rsi/57/8?ver=pdfcov>

Published by the [AIP Publishing](#)

Articles you may be interested in

[Describing Single Proteins Located In Membrane Structures by TERS](#)

AIP Conf. Proc. **1267**, 1235 (2010); 10.1063/1.3482399

[Pore nucleation in mechanically stretched bilayer membranes](#)

J. Chem. Phys. **123**, 154701 (2005); 10.1063/1.2060666

[Pore formation in fluctuating membranes](#)

J. Chem. Phys. **122**, 044901 (2005); 10.1063/1.1835952

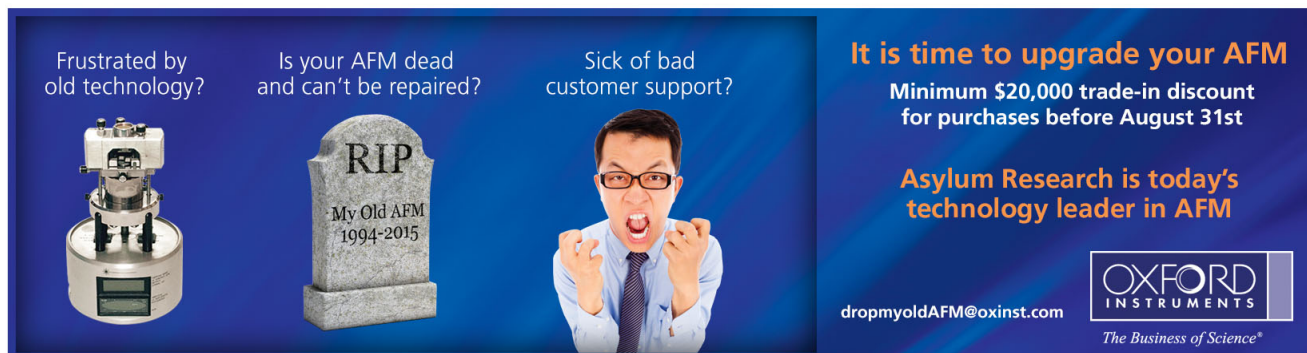
[Preparation and photoluminescence of alumina membranes with ordered pore arrays](#)

Appl. Phys. Lett. **74**, 2951 (1999); 10.1063/1.123976

[Manufacturing and testing VLPC hybrids](#)

AIP Conf. Proc. **450**, 361 (1998); 10.1063/1.56979

Frustrated by old technology? Is your AFM dead and can't be repaired? Sick of bad customer support?



It is time to upgrade your AFM
Minimum \$20,000 trade-in discount for purchases before August 31st

Asylum Research is today's technology leader in AFM

dropmyoldAFM@oxinst.com

OXFORD INSTRUMENTS
The Business of Science®

Manufacture, observation, and test of membranes with locatable single pores

R. E. Packard

Department of Physics, University of California, Berkeley, California 94720

J. P. Pekola^{a)}

Low Temperature Laboratory, Helsinki University of Technology, SF-02150, Espoo 15, Finland

P. B. Price

Department of Physics, University of California, Berkeley, California 94720

R. N. R. Spohr^{b)}

Gesellschaft fuer Schwerionenforschung, D-6100 Darmstadt, Federal Republic of Germany

K. H. Westmacott

Materials and Molecular Research Division, Lawrence Berkeley Laboratory, Berkeley, California 94720

Zhu Yu-Qun^{c)}

Low Temperature Laboratory, Huazhong University of Science and Technology, Wuhan, Hubei, The People's Republic of China

(Received 5 March 1986; accepted for publication 5 May 1986)

A method for generating single pores down to $0.1 \mu\text{m}$ diameter in the center of a large circular foil is described, based on nuclear tracks. The foil is framed by a tension ring which enables one to handle the foils in a well-defined precise way. The single pore has a lateral displacement of ± 0.1 mm with respect to the tension ring center. The foils used are polycarbonate of the type Makrofol and have thicknesses between 2 and $10 \mu\text{m}$. For calibration of the single pore diameters, multiple nuclear tracks between 0.1 and $3.5 \mu\text{m}$ diameter are etched and observed by microscopy. The microscopic observations are compared with gas-flow measurements, using two alternative methods: multiple holes are tested under viscous flow conditions of N_2 gas at normal temperature and pressure; single holes are tested under collisionless flow conditions of ^4He gas at liquid-nitrogen temperature, using a capacitance method.

INTRODUCTION

Single-pore membranes have previously been used as counting apertures for measuring number, size, and mobility of particles in aqueous suspensions.¹ In the past few years, they have also been used to study the deformability of individual red blood cells with implications in diagnostic medicine and pharmacology.² More recently, a promising application of such pores in the field of low-temperature physics appeared. In this field, single-pore membranes with a simple geometry and with diameters smaller than $0.5 \mu\text{m}$ are needed to study the critical-flow behavior of superfluid ^3He at sub-millikelvin temperatures. With single-pore membranes, two basic experiments may be performed:

(1) Observation of phase slip centers in superfluid ^3He , combined with the indirect observation of the Josephson effect. This requires single pores with diameters $d \leq 0.5 \mu\text{m}$ and lengths $L \cong 5 \mu\text{m}$. Such pores can be manufactured according to the technique of our present report.

(2) Direct observation of the Josephson effect in superfluid ^3He . This requires a weak link, i.e., a pore with a diameter $d \cong 0.05 \mu\text{m}$, and a length $L \cong 0.05 \mu\text{m}$, which is smaller than the coherence length of the Cooper pairs in superfluid

^3He . Such pores cannot be manufactured by the technique described here, but their diameter is still well above the present limit of the nuclear track technique³ of about $0.01 \mu\text{m}$.

The suggested low-temperature experiments depend crucially on the controlled manufacture of locatable single pores in the diameter range between about 1 and $0.01 \mu\text{m}$. With this goal in mind, we developed a technique for precise handling of thin foils between 2 and $10 \mu\text{m}$ and localized generation of single pores with diameters between 0.1 and $3.5 \mu\text{m}$.

I. PREPARATION TECHNIQUE

A. Foil material

During the past few years, $30\text{-}\mu\text{m}$ Makrofol⁴ N yellow had been successfully used for manufacturing about 10 000 almost cylindrical pores⁵ with diameters of $4.0 \pm 0.08 \mu\text{m}$ for studying the deformability of red blood cells. Due to the high homogeneity of Makrofol N, pore sizes varied only of the order of 2% for these pores. Unfortunately, this material is not available in thicknesses below $20 \mu\text{m}$. Therefore, we used the next best alternative, Makrofol SKG blue,⁶ which is available in suitable thicknesses of 2.0- and $6.0\text{-}\mu\text{m}$ -thick

foils. Makrofol SKG blue is a cast film, longitudinally stretched and crystallized. The two sides of the foil have a different surface structure. One side is smooth, the other is rough. Compared with Makrofol N yellow, which is a cast film of high homogeneity and amorphousness, the track etch properties of Makrofol SKG blue are inferior, but still it is a fair choice for first experiments.

In a separate track etch test, a laminated double foil consisting of 6.0- μm Makrofol SKG blue and 2.3- μm Makrofol KG green was also employed. This foil is obtained by welding the two foils together while they are pulled over a heated aluminum block which is kept at a temperature of 220 °C. In the future, such a double layer material may provide the possibility for creating very small nuclear track holes in a thin foil with low bulk etch rate, supported by a thick foil with high bulk etch rate. As it happened, in our test case, the untreated materials Makrofol SKG and KG have approximately the same bulk etch rates.

B. Foil framing and centering

For generating single-pore membranes with a defined location of the hole, it is necessary to attach a frame rigidly to the delicate foil. In this way, the pore can be kept centered throughout all steps of the preparation, i.e., from the single-particle irradiation to an eventual application in low-temperature experiments. And after the experiments, the single pore can be relocated and finally and destructively inspected with high-resolution methods. For this purpose, the foil is stretched over a tension ring and centered with respect to the beam aperture of the irradiation device (Fig. 1). This procedure consists of the following steps.

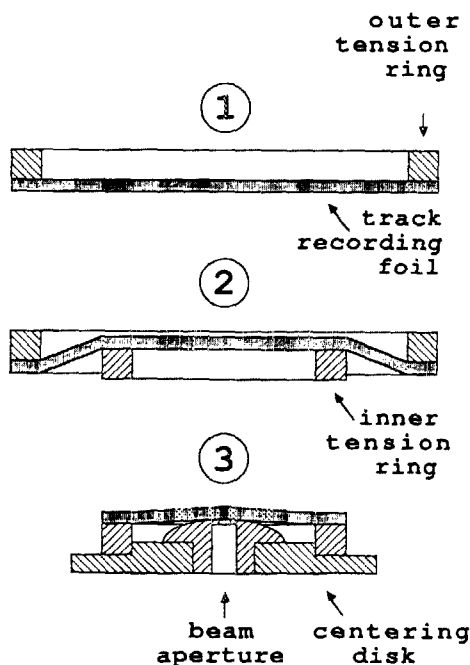


FIG. 1. Foil framing and centering. (1) The foil is glued to the outer tension ring. (2) The pretensioned foil is epoxied to the inner tension ring. The weight of the outer tension ring defines the tautness of the foil. (3) The framed foil is centered to the irradiation system.

1. Mounting the foil to the outer tension ring

The foil material, as obtained, consists of a stack of several foils in standard paper sheet size. To overcome the mutual electrostatic attraction between the foils in the stack and the tendency of individual foils to collapse after separation onto themselves, a standard size paper sheet is placed in direct contact with the foil stack and the uppermost foil is removed together with this overlayer sheet from the stack. The separated foil is placed together with its supporting paper sheet on a flat surface, whereby the foil is on top. For later observation with a light microscope, the shiny side of the foil becomes the topmost surface. This improves the observation of pores, especially if reflected-light objectives are used in the light microscope. Double adhesive tape or rapidly solidifying epoxy,⁷ slightly thinned by trichloroethane for smoother brushing and prolonged pot life, is used to cement the foil to the outer tension ring (top of Fig. 1). The outer tension ring is located, with respect to the foil sheet, so that a critical zone around the center of the ring of about 2 cm diameter has as few visible defects as possible. Defects in the form of tiny indents can be observed in reflected light. Once mounted on the outer tension ring, the foil can be handled unsupported. It is, however, still somewhat floppy and not completely taut.

2. Mounting the inner tension ring

The inner tension ring (stainless-steel type 304, NaOH resistant) is cemented to the pretensioned foil roughly centered, using unthinned epoxy. The weight of the outer tension ring (or additional rings if desired) defines the force of tension (middle of Fig. 1).

3. Centering of the framed foil to the irradiation system

After the epoxy has hardened, the foil is cut between the inner and the outer tension ring and inserted into the centering disk of the irradiation device (bottom of Fig. 1). The polished upper surface of the beam aperture protrudes somewhat over the upper surface of the inner tension ring, leading to a direct contact between the foil and the beam-defining aperture. For single-pore membranes, a 0.1-mm-diam aperture, and for multipore membranes, a 1.0-mm-diam aperture, is used. The foil center coincides with the center of the beam aperture to within ± 0.1 mm. In this way, etched single pores, down to about 0.3 μm diameter, can later be verified and inspected repeatedly using a light microscope. For recycling used foil rings, foil and epoxy remains are removed after soaking in a mixture of methylene chloride and phenol.⁸

C. Irradiation

For irradiation, a ²⁵²Cf fission fragment source (e.g., Ref. 9) of nominal strength 5 μCi (half-life 2.64 years) is used. In polycarbonate, the average range of the fission fragments is about 22 μm . Since the range distribution is quite broad, however, thicker foils may lead to an appreciable number of unregistered track events, already at thicknesses

$L \gg 10 \mu\text{m}$. The actual strength of the 3-mm-diam fission source (age: about 2.5 years) at 10 mm distance was about 400 fission fragments per second and square centimeter and at 39 mm distance, which is the actual distance between the source and the irradiated foil, about 26 fission fragments per second per square centimeter. The simultaneously emitted alpha particles normally do not lead to perforated nuclear tracks in Makrofol, due to their much lower track etch rate. Only at very long etch times may alpha tracks eventually perforate the foils. They occur at about 20 times higher rate and can be electronically discriminated against the fission fragments for foils with thicknesses $L \leq 10 \mu\text{m}$.

The irradiation system (Fig. 2) uses an electromechanical shutter which switches the beam off, as soon as a preset number of fission fragments has passed through the track recording foil and been detected in a silicon surface-barrier particle detector.¹⁰ As beam-defining aperture, a mechanically drilled, electropolished hole of 0.1 mm diameter in a stainless-steel plate of 0.25 mm original thickness is used. The beam aperture is central within ± 0.1 mm with respect to the inner tension ring. For discrimination against the registration of the alpha particles by the preset counter, the single-channel analyzer is set just above the alpha peak, using for this adjustment a multichannel analyzer in connection with a test pulse generator and an oscilloscope. With the 0.1-mm-diam beam aperture, at the average about one fission fragment is registered every 8 min in the preset counter. For generating multipore membranes, a beam aperture of hundred times larger area (diameter $d = 1$ mm) is inserted in the centering disk.

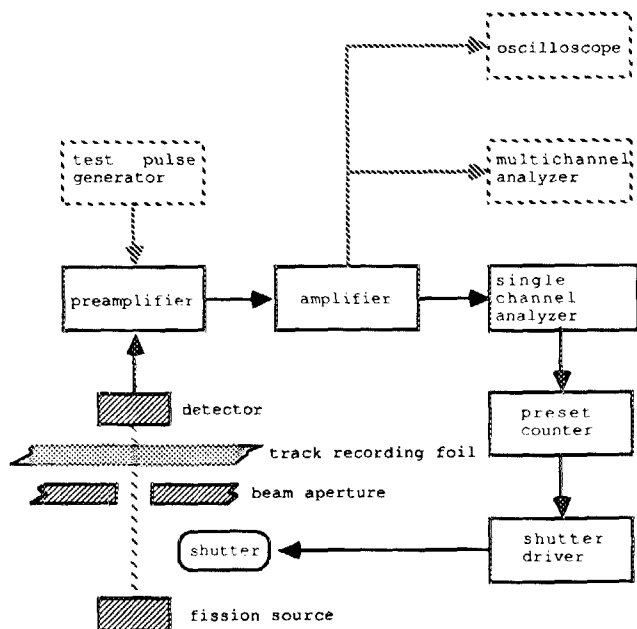


FIG. 2. Irradiation system. Fission fragments from a ^{252}Cf source are collimated by the beam aperture. They penetrate through the track recording foil and are detected by a particle detector. The resulting signal is amplified. A single-channel analyzer discriminates against low-energy alpha particles from the same source. Alpha particles are about 20 times more abundant but normally do not lead to etched pores. A preset counter counts the fission fragment events and activates the electromechanical shutter as soon as the preset number is reached. A test pulse generator in connection with a multichannel analyzer serves for adjusting the single-channel analyzer just above the alpha-peak energy.

D. Etching

As etching medium 6.25 *n* NaOH solution is used. The influence of the addition of 0.04% Dowfax 2A1 surfactant¹¹ to the etching medium on the etch rate was tested. Dowfax 2A1 contains about 50% sodium mono- and di-dodecyl disulfonated diphenyloxide and seems to react chemically with the NaOH solution, indicated by a slightly milky appearance of the resulting etching medium. The etching bath is kept at 70 °C. The inner tension rings, carrying the irradiated foils, are hung into the etching bath, using a stainless-steel bolt which is screwed axially into the tension ring.

At the desired etch time, the etching process is interrupted and the foil rings are flushed for about 30 min in running tap water. Then the membranes are flushed either with isopropanol (for microscopic observations) or with a spray of distilled water (for gas-flow measurements) and finally dried using a gas spray.¹² Flushing is always performed on both sides of the membranes, starting from the center of the membrane to push etch residues away from the nuclear track holes.

II. OBSERVATION OF PORES

A. Microscopic observations

1. Light microscopy

For observation of etched nuclear tracks down to 0.3 μm diameter, the light microscope is used in transmitted-light dark-field illumination mode. The tracks can be visually distinguished from surface roughnesses and impurities by their characteristic diffraction patterns and can be followed throughout the thickness of the foil. For microscopic observation of single pores, a centering disk (bottom of Fig. 1) with a central aperture of 1 mm diameter is used as the search window. In this way, single pores can be repeatedly located, even after additional etch procedures, as long as the tension ring remains attached to the foil. Also, double pores or faulty membranes with no pores at all can be identified and eliminated, and the proper electronic discrimination setting of the irradiation device checked. Only for pores with sufficiently large diameters $d \gg 1 \mu\text{m}$, a rough estimate for the pore size can be obtained in this way, using the light microscope.

2. Scanning electron microscopy

Scanning electron microscopy has been used in a few cases to check the roughness of the pore walls and control the obtained pore shapes and sizes. In comparison to the previously mentioned nuclear track holes in Makrofol N yellow, a much inferior pore geometry is achieved. The pore cross section is frequently slightly elliptical due to the longitudinal stretching of the raw material. Also, frequent irregularities of the pore edges are observed. Scanning electron microscopy always shows a sharp cutoff of the density profile at the boundary of the material.

3. Transmission electron microscopy

High-voltage transmission electron microscopy is used to observe etched tracks directly and determine the pore di-

ameters down to less than $0.1\ \mu\text{m}$. It enables the direct observation of etched pores in thick samples up to about $6\ \mu\text{m}$ without any further replication techniques.

Sample preparation: This requires manipulation under a stereo microscope. Its main step is the transfer of the etched-track zone in the center of the tensioned membrane onto the TEM grid. The grid consists of copper, has a diameter of 3 mm, and about one line per $0.5\ \text{mm}$. Five-minute epoxy is thinned, using trichloromethane as a rapidly vaporizing plasticizer. A drop is put on cardboard paper under the stereo microscope. The TEM grid is pulled through the drop, using a preparation needle. The lower side of the copper grid is dried by pulling it over the cardboard. Most of the glue on the top side is removed by a scalpel. The scalpel is attached to the outermost boundary of the TEM grid. The grid is placed in the center of the framed foil, using a centering disk (Fig. 1, bottom). The grid is slightly pressed onto the foil with the scalpel, to obtain full contact between epoxy and foil. The assembly is removed from the centering disk. After the epoxy has polymerized, the grid, together with its nuclear track foil, is cut out by circumcission, using a scalpel.

The firm attachment of the foil to the TEM grid has two benefits. First, the flatness and tension of the foil is maintained during the transfer. Second, good thermal contact

between the foil and the TEM grid is obtained in this way, thus reducing the problem of foil heating and thermoplastic deformation of the etched tracks in the transmission electron microscope.

The mounted TEM samples are observed without further conductive coating in the high-voltage electron microscope at 1.5-MeV acceleration voltage. Using a high-voltage microscope enables one to directly view samples, up to a thickness of $6\ \mu\text{m}$, and still observe tracks down to $d \leq 0.4\ \mu\text{m}$ diameter. In $2\text{-}\mu\text{m}$ -thick material, the smallest observed pore diameter is still smaller with $d < 0.1\ \mu\text{m}$. Below this size, the contrast of the etched material becomes insufficient due to electron scattering in the foil.

In this way, an overall view of the projected areal density of the material after track etching can be obtained. The TEM observations show that the etching process attacks the crystalline material unevenly, yielding diffuse pore geometries, especially for overetched samples when the ratio between the pore diameter and the thickness of the remaining material approaches 1 (Fig. 3). The addition of the surfactant 2A1 improves the smoothness of the pores somewhat. Pores with diameters smaller than about $0.1\ \mu\text{m}$ cannot be directly observed, due to lacking contrast, even for the thinnest foil used here, the $2.0\text{-}\mu\text{m}$ -thick Makrofol SKG blue. Figure 4 shows a "good" nuclear track pore in $6.0\text{-}\mu\text{m}$

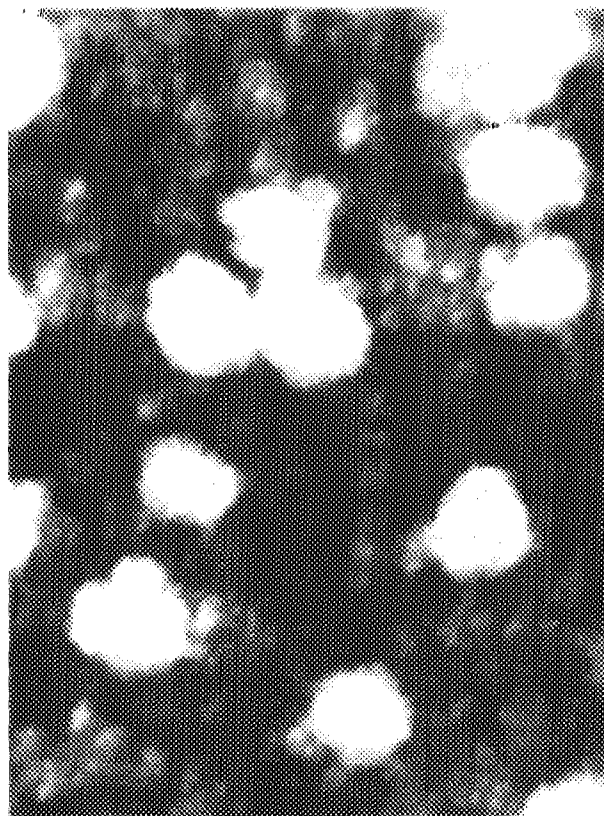


FIG. 3. Transmission electron micrograph of over-etched pores. Material: $2.0\text{-}\mu\text{m}$ -thick Makrofol SKG blue. Irradiation: about 10^6 fission fragments per cm^2 . Etching: $6.25\ n$ NaOH at $70\ ^\circ\text{C}$, 16 min. Observation: high-voltage transmission electron microscopy, direct mode without further preparation steps. Pore diameter: $1.3 \pm 0.2\ \mu\text{m}$. Bulk etch rate: $2.4\ \mu\text{m}/\text{h}$. The pores are very diffuse due to the prolonged etching of the crystalline material. Thinner parts of the foil have already etched through. The small pores are possibly due to alpha tracks.

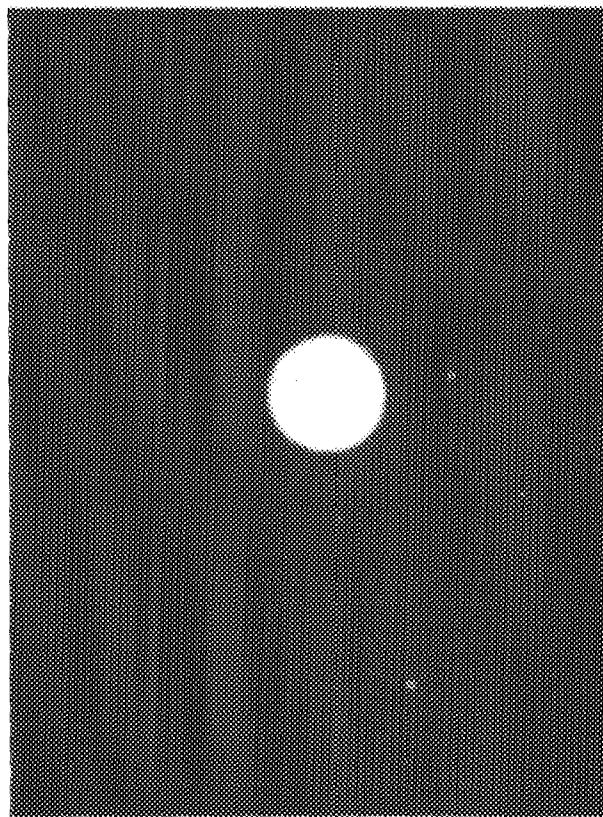


FIG. 4. Transmission electron micrograph of a "good" pore. Material: $6.0\text{-}\mu\text{m}$ -thick Makrofol SKG blue. Irradiation: About 10^6 fission fragments per cm^2 . Etching: $6.25\ n$ NaOH at $70\ ^\circ\text{C}$, 4 min. Observation: high-voltage transmission electron microscopy, direct mode without further preparation steps. Pore diameter: $0.41\ \mu\text{m}$. Bulk etch rate: $3.1\ \mu\text{m}/\text{h}$. The pore diameter increases at twice the bulk etch rate.

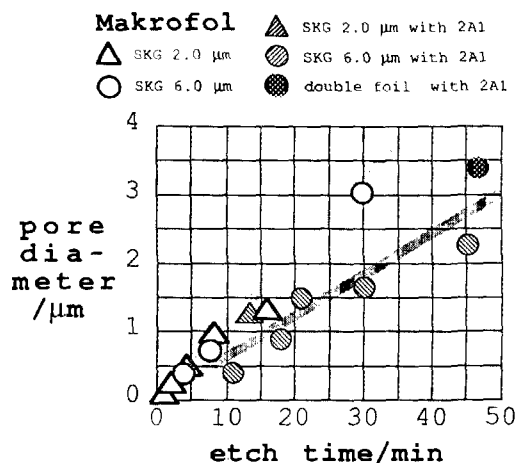


FIG. 5. Pore-diameter calibration. The etched pore diameters depend on the presence of 0.04% Dowfax 2A1 surfactant in the etching medium (6.25 n NaOH at 70 °C). Upper data points: without 2A1 (open symbols). Lower data points: with 2A1 (shaded symbols). The data points correspond to Table I. As expected, the nuclear track diameters grow about linearly with time. However, it is surprising that the surfactant reduces the bulk etch rate.

Makrofol SKG blue with a diameter of 0.41 μm. This pore is obtained by etching the irradiated foil for 4 min in 6.25 n NaOH without surfactant at 70 °C. Its bulk etch rate is 3.1 μm/h.

Figure 5 shows the influence of the surfactant on the speed of the etching process. The data points correspond to the values given in Table I. Figure 6 is a different representation of the same data showing the independence of the average bulk etch rate of the pore diameter (or etch time).

B. Gas-flow measurements

Two methods based on gas flow are employed to determine effective pore sizes. The pressure, temperature, and sample gas are chosen such that the flow regime is either of the viscous or of the collisionless type.

We use N₂ gas at normal temperature and pressure to study the viscous flow through multipore membranes. We

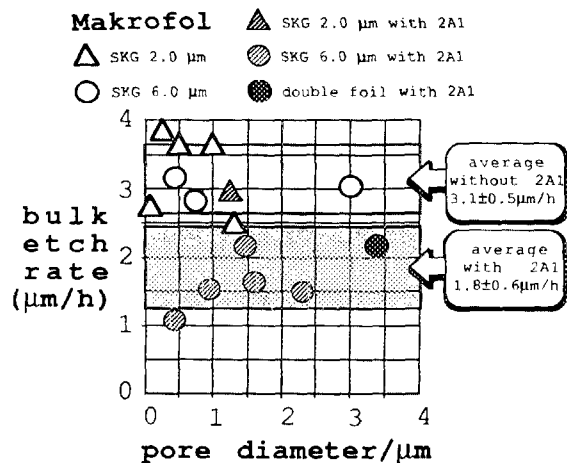


FIG. 6. Determination of bulk etch rates. Demonstration of the independence of the bulk-etch rate on the track diameter (or etch time). Without the surfactant 2A1 (open symbols), the average bulk etch rate is 3.1 ± 0.5 μm/h. With 0.04% surfactant 2A1 added (shaded symbols), the average bulk etch rate is 1.8 ± 0.6 μm/h. The data points correspond to Table I.

use ⁴He gas at liquid-nitrogen temperature (77 K) to study the collisionless flow through single-pore membranes. In both cases, the pores are generated in 6.0-μm Makrofol, using 6.25 n NaOH + 0.04% surfactant 2A1 at 70 °C.

1. Viscous flow

For N₂ gas at normal temperature and pressure, the mean free path $l \approx 0.1 \mu\text{m}$ (see, e.g., Ref. 13), well below the diameter of the holes studied in the viscous flow regime. The volume flow rate dV/dt through N holes with diameter d and length L with a pressure difference ΔP is then given by

$$\frac{dV}{dt} = \left(\frac{N\pi d^4}{128L\eta} \right) \Delta P,$$

where η is the viscosity of the gas flowing through the pores into a cylindrical cavity (Fig. 7). The flow is observed by the capacitive detection method (see, e.g., Ref. 14). The dis-

TABLE I. Makrofol etch rates from microscopic observation.

Material	Etch time/min	Etchant	Etch Temp/°C	Pore diameter/μm	Bulk etch rate (μm/h)
Makrofol SKG blue, 2.0 μm	1,0	6.25nNaOH	70	0,09	2,7
	2,0	6.25nNaOH	70	0,25	3,8
	4,0	6.25nNaOH	70	0,48	3,6
	8,0	6.25nNaOH	70	0,96	3,6
	13,0	6.25nNaOH + 2A1	70	1,25	2,9
	16,0	6.25nNaOH	70	1,30	2,4
Makrofol SKG blue, 6.0 μm	4,0	6.25nNaOH	70	0,43	3,2
	8,0	6.25nNaOH	70	0,74	2,8
	11,0	6.25nNaOH + 2A1	70	0,41	1,1
	18,0	6.25nNaOH + 2A1	70	0,90	1,5
	21,0	6.25nNaOH + 2A1	70	1,50	2,1
	30,0	6.25nNaOH	70	3,04	3,0
	45,0	6.25nNaOH + 2A1	70	1,60	1,6
Makrofol SKG + KG, double foil	45,0	6.25nNaOH + 2A1	70	2,30	1,5
	47,0	6.25nNaOH + 2A1	70	3,40	2,2

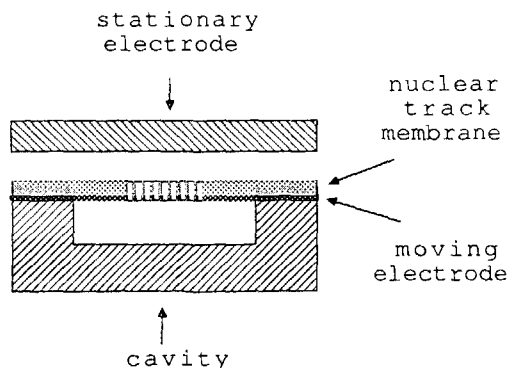


FIG. 7. Device for measurement of viscous flow through multipore membranes. At $t = 0$ a voltage V is put between the two electrodes. The membrane bulges upward to a position x_0 , creating a pressure difference $-\Delta P$ between the inside and outside of the cavity. The exponential relaxation of the membrane from position x_0 to a higher position x_∞ , as it fills up with gas, is measured as function of time, by measuring the capacitance of the two-electrode system with a capacitance bridge using a lock-in amplifier.

placement x of the porous membrane with respect to the equilibrium position at $\Delta P = 0$ and zero voltage between the electrodes is proportional to the change of the capacitance between the stationary drive electrode and the moving membrane electrode. It is given by

$$x = x_\infty [1 - (1 - x_0/x_\infty) \exp(-t/\tau)],$$

where x_0 is the displacement at $t = 0$, when the dc voltage is switched on, creating a finite pressure difference across the pores, and x_∞ is the displacement for $t = \infty$, when this pressure difference has again decreased to 0. The relaxation time τ is given by

$$\tau = (128L\eta/N\pi d^4)A/\lambda,$$

where A is the area of the moving membrane and λ is its elastic restoring constant, defined by the equation $x = \Delta P/\lambda$. The resulting pore diameter d for different etching times, deduced from measured relaxation times τ , is given in Table II. The given standard deviation for the collisionless flow experiments gives the repeatability after thermal cycling up to room temperature and again down to liquid-nitrogen temperature.

2. Collisionless flow

Figure 8 shows the device for collisionless gas-flow measurements through a single-pore membrane. Due to its

TABLE II. Effective pore diameters from gas flow measurements.

Etch time /min	Number of holes	Flow conditions	Eff. pore diameter / μm	Std. dev. / μm
15	1.000	viscous	0,33	—
18	1	collisionless	0,44	0.02
18	1	collisionless	0,52	0.06
20	10	viscous	0,7	—
30	1.000	viscous	1,1	—
45	1.000	viscous	1,8	—

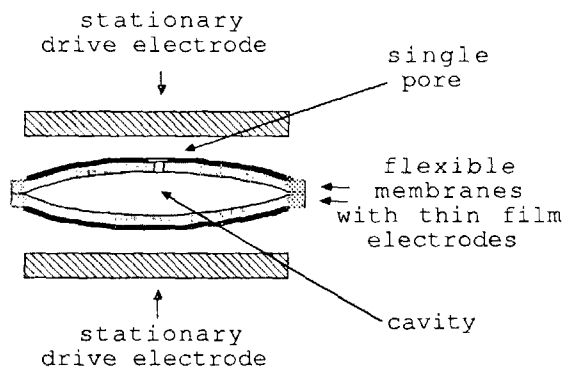


FIG. 8. Device for measurement of collisionless flow through single-pore membranes. For measuring the gas transport through single pores, a gas cell consisting of two hermetically sealed membranes is used. One of the membranes carries the single pore. Both membranes carry on their outside a thin-film electrode. The drive electrodes are used to induce a suitable electrostatic force on the flexible membrane electrodes, between which the capacitance is measured. The device is characterized by a very small volume of the cavity and a high capacitance between the inner electrodes and is suited for measuring the collisionless flow through single-pore membranes with diameters $d < 1 \mu\text{m}$.

smaller cavity and the increased capacitance between the flexible membrane electrodes this device has increased sensitivity. Again, the capacitive detection method for displacement is employed to measure the distance between the two flexible single-pore membranes, forming a sealed cavity.

The mean free path of ^4He gas at 77 K is $l \approx 0.07 \mu\text{m}/P$, where P is the ambient pressure measured in atmospheres. Thus at sufficiently low pressures ($P < 0.01$ atm), the flow through submicron size pores is in the collisionless regime and the mass transport through a long cylindrical pore is given by^{15,16}

$$\frac{dm}{dt} = \left(\frac{\pi d^3}{4\bar{v}L} \right) \Delta P,$$

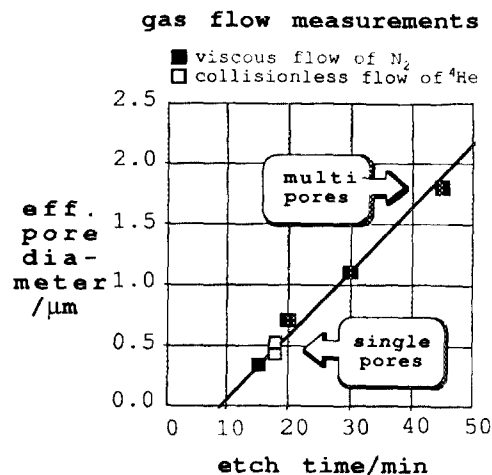


FIG. 9. Gas-flow measurements. Calculated pore diameters from gas-flow measurements using the gas cells of Figs. 7 and 8. All pores are in 6.0- μm Makrofol SKG, etched in 6.25 n NaOH + 0.04% surfactant 2A1 at 70 $^\circ\text{C}$. The line through the measured points intercepts the x axis at around 8 min. This may be due to improper foil cleaning after the track etching procedure.

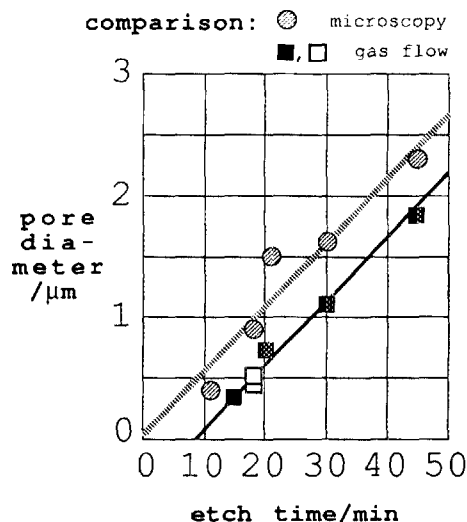


FIG. 10. Comparison between microscopy and gas-flow measurements. Only observations for 6.0- μm Makrofol SKG blue, etched with surfactant 2A1, are shown. The shift between the microscopic and the gas-flow measurements is about 0.4 μm . It may be due to different flushing procedures or shrinkage of the pores during the preparation of the gas cells, e.g., during the evaporation of the thin-film electrodes. To verify this, the membranes must ultimately be observed by electron microscopy after the gas-flow measurements have been completed.

where \bar{v} is the root mean square velocity of the gas molecules. This leads to the exponential relaxation time for flow to or from the cavity, given by

$$\tau = \left(\frac{4\sqrt{3}}{\pi} \right) \left(\frac{VL}{d^3} \right) \left(\frac{m}{kT} \right)^{1/2},$$

where V is the volume of the sealed cavity, m is the mass of the gas molecule ($= {}^4\text{He}$ atom), k is the Boltzmann constant, and T is the temperature.

III. RESULTS

A. Microscopic observations

From the different microscopic observations pore diameters and bulk etch rates are determined (Table I). The average bulk etch rate for 2.0- μm Makrofol SKG blue is $3.2 \pm 0.6 \mu\text{m}/\text{h}$. It is $2.4 \pm 0.9 \mu\text{m}/\text{h}$ for 6.0- μm Makrofol SKG blue. For the double-foil Makrofol SKG and KG with an approximate thickness of 10 μm it is 2.2 $\mu\text{m}/\text{h}$.

The surfactant reduces the bulk etch rate by a factor of about 1.7.

B. Gas-flow measurements

Figure 9 suggests a linear relation between the etch time and the effective pore diameter as deduced from measured relaxation times. All pores are in 6.0- μm Makrofol SKG, etched in 6.25 n NaOH + 0.04% surfactant 2A1 at 70 $^\circ\text{C}$. Its data points are separately listed in Table II.

C. Comparison

In Fig. 10, the microscopic observations are compared with the gas-flow measurements. Only pores in 6.0- μm Makrofol SKG, etched in 6.25 n NaOH + 0.04% surfactant 2A1 at 70 $^\circ\text{C}$ are considered. According to the microscopic observation, the pore diameters grow at a rate of about 3.1 $\mu\text{m}/\text{h}$. There exists a marked shift between the microscopic and the gas-flow measurements of about 0.4 μm . We attribute it to the different flushing procedures mentioned above. Another possible explanation for the shift could be shrinking of the pores during the preparation of the gas cells (e.g., during the evaporation of the metal electrodes). The extrapolated curve shows that pores with etch times shorter than 8 min, flushed with water, apparently collapse during the preparation of the gas cells. In the future, therefore, electron microscopic observations have to be performed after gas-flow measurements. The microscopic observations follow the equation $d[\mu\text{m}] \cong 3.14t[\text{h}] + 0.03$. The gas flow measurements follow the equation $d[\mu\text{m}] \cong 2.90t[\text{h}] - 0.36$.

ACKNOWLEDGMENTS

This work has been supported in part by the Nuclear Physics Division of the Lawrence Berkeley Laboratory, Berkeley, CA 94720. This work was also supported by the National Science Foundation—Low Temperature Physics—Grant DMR 8516905.

- ^{a)} Visiting scientist at University of California, Berkeley.
- ^{b)} Visiting scientist at Lawrence Berkeley Laboratory, Berkeley, California 94720.
- ^{c)} Visiting scientist at University of California, Berkeley.
- ¹R. W. DeBlois, C. P. Bean, and R. K. A. Wesley, *Colloid Interface Sci.* **61**, 323 (1977).
- ²H. G. Roggenkamp, H. Kiesewetter, R. Spohr, U. Dauer, and L. C. Busch, *Biomed. Tech.* **26**, 167 (1981).
- ³R. L. Fleischer, P. B. Price, and R. M. Walker, *Univ. of California, Berkeley*, 1975.
- ⁴Bayer AG, Leverkusen, FRG.
- ⁵W. Czilwa, E. Pfeng, R. Spohr, and J. Vetter, *GSI Annual Report 1985*, GSI, Darmstadt, FRG.
- ⁶G. Schexnayder, Mobay Chemical Co., Pittsburgh, PA 15205, phone (412) 777-2833.
- ⁷Five-Minute Epoxy, Hardman, Inc., Belleville, NJ 07109, phone (201) 751-3000.
- ⁸Strip-X, GC Electronics, Rockford, IL 61101.
- ⁹Amersham, Radiochemical Centre, Ltd., White Lion Road, Amersham, Buckinghamshire, HP7 9LL, U.K.
- ¹⁰Ortec, Oak Ridge, TN.
- ¹¹Dowfax 2A1 solution, Dow Chemical Co., Midland, MI 48640.
- ¹²Aero Duster, Miller Stephenson Chemical Co., Inc., Danbury, CT 06810.
- ¹³F. Reif, *Fundamentals of Statistical and Thermal Physics* (McGraw-Hill, New York, 1965).
- ¹⁴M. T. Manninen and J. P. Pekola, *J. Low Temp. Phys.* **52**, 497 (1983).
- ¹⁵M. Knudsen, *Ann. Phys.* **28**, 75 (1909).
- ¹⁶E. M. Sparrow, V. K. Jonsson, and T. S. Lundgren, *J. Heat Transfer*, 111 (May 1963).